AJNR

MR Imaging–Based Radiomic Signatures of Distinct Molecular Subgroups of Medulloblastoma

M. Iv, M. Zhou, K. Shpanskaya, S. Perreault, Z. Wang, E. Tranvinh, B. Lanzman, S. Vajapeyam, N.A. Vitanza, P.G. Fisher, Y.J. Cho, S. Laughlin, V. Ramaswamy, M.D. Taylor, S.H. Cheshier, G.A. Grant, T. Young Poussaint, O. Gevaert and K.W. Yeom

AJNR Am J Neuroradiol published online 6 December 2018
http://www.ajnr.org/content/early/2018/12/06/ajnr.A5899

Published December 6, 2018 as 10.3174/ajnr.A5899

MR Imaging–Based Radiomic Signatures of Distinct Molecular Subgroups of Medulloblastoma

M. Iv, M. Zhou, K. Shpanskaya, S. Perreault, Z. Wang, E. Tranvinh, B. Lanzman, S. Vajapeyam, N.A. Vitanza, P.G. Fisher, Y.J. Cho, S. Laughlin, V. Ramaswamy, M.D. Taylor, S.H. Cheshier, G.A. Grant, T. Young Poussaint, O. Gevaert, and K.W. Yeom

ABSTRACT

BACKGROUND AND PURPOSE: Distinct molecular subgroups of pediatric medulloblastoma confer important differences in prognosis and therapy. Currently, tissue sampling is the only method to obtain information for classification. Our goal was to develop and validate radiomic and machine learning approaches for predicting molecular subgroups of pediatric medulloblastoma.

MATERIALS AND METHODS: In this multi-institutional retrospective study, we evaluated MR imaging datasets of 109 pediatric patients with medulloblastoma from 3 children's hospitals from January 2001 to January 2014. A computational framework was developed to extract MR imaging–based radiomic features from tumor segmentations, and we tested 2 predictive models: a double 10-fold cross-validation using a combined dataset consisting of all 3 patient cohorts and a 3-dataset cross-validation, in which training was performed on 2 cohorts and testing was performed on the third independent cohort. We used the Wilcoxon rank sum test for feature selection with assessment of area under the receiver operating characteristic curve to evaluate model performance.

RESULTS: Of 590 MR imaging–derived radiomic features, including intensity-based histograms, tumor edge-sharpness, Gabor features, and local area integral invariant features, extracted from imaging-derived tumor segmentations, tumor edge-sharpness was most useful for predicting sonic hedgehog and group 4 tumors. Receiver operating characteristic analysis revealed superior performance of the double 10-fold cross-validation model for predicting sonic hedgehog, group 3, and group 4 tumors when using combined T1- and T2-weighted images (area under the curve = 0.79, 0.70, and 0.83, respectively). With the independent 3-dataset cross-validation strategy, select radiomic features were predictive of sonic hedgehog (area under the curve = 0.70–0.73) and group 4 (area under the curve = 0.76–0.80) medulloblastoma.

CONCLUSIONS: This study provides proof-of-concept results for the application of radiomic and machine learning approaches to a multi-institutional dataset for the prediction of medulloblastoma subgroups.

ABBREVIATIONS: AUC = area under the curve; LAII = local area integral invariant; MB = medulloblastoma; ROC = receiver operating characteristic; SHH = sonic hedgehog; SVM = support vector machines; WNT = wingless type

Medulloblastoma (MB) is the most common malignant brain tumor in children and a leading cause of cancer-related morbidity and mortality in this population.[1] Although once considered a single tumor type, recent molecular advances have identified at least 4 biologically distinct subgroups of MB (sonic hedgehog [SHH],

Received June 29, 2018; accepted after revision October 6.

From the Department of Radiology (M.I., M.Z., K.S., E.T., B.L., K.W.Y.), Department of Pediatrics (P.G.F.), Pediatric Neurology, and Department of Neurosurgery (G.A.G.), Pediatric Neurosurgery, Lucile Packard Children's Hospital, Stanford University, Palo Alto, California; Stanford Center for Biomedical Informatics (M.Z., O.G., Z.W.) and Department of Radiology (K.W.Y.), Artificial Intelligence in Medicine and Imaging, Stanford University, Stanford, California; Department of Pediatrics (S.P.), Pediatric Neurology, Centre Hospitalier Universitaire Sainte Justine, University of Montréal, Montreal, Quebec, Canada; Department of Radiology (S.V., T.Y.P.), Boston Children's Hospital, Harvard University, Boston, Massachusetts; Department Pediatrics Hematology-Oncology (N.A.V.), Seattle Children's Hospital, University of Washington, Seattle, Washington; Department of Pediatrics (Y.J.C.), Pediatric Neurology, Oregon Health & Science University, Portland, Oregon; Departments of Radiology, Neuro-Oncology, and Neurosurgery (S.L., V.R., M.D.T.), Hospital for Sick Children, Toronto, Ontario, Canada; and Department of Neurosurgery (S.H.C.), Pediatric Neurosurgery, University of Utah, Salt Lake City, Utah.

Michael Iv and Mu Zhou are co-first authors and contributed equally to this article.

Kristen W. Yeom and Olivier Gevaert are co-senior and co-corresponding authors and contributed equally to this article.

Research reported in this publication was supported by the National Institute of Biomedical Imaging and Bioengineering of the National Institutes of Health under Award Number R01EB020527. V.R. was supported by the collaborative ependymoma research network.

The content of this article is solely the responsibility of the authors and does not necessarily represent the official views of the National Institutes of Health.

Please address correspondence to Kristen W. Yeom, MD, Lucile Packard Children's Hospital, Stanford University Medical Center, Department of Radiology, Pediatric MRI and CT, Room 0511, 725 Welch Rd, Palo Alto, CA 94304; e-mail: kyeom@stanford.edu.

Indicates open access to non-subscribers at www.ajnr.org

Indicates article with supplemental on-line tables.

Indicates article with supplemental on-line photos.

http://dx.doi.org/10.3174/ajnr.A5899

Table 1: Patient demographics

Characteristic	Institutional Cohort		
	Stanford	Boston	Toronto
No. of patients	32	28	49
Age (mean) (yr)	10.14 ± 8.49	8.54 ± 4.52	7.53 ± 3.69
Male sex (No.) (%)	23 (72)	9 (32)	32 (65)
Molecular subgroup (No.)			
SHH	11	9	10
WNT	4	5	10
Group 3	7	5	12
Group 4	10	9	17
MRI availability (No.)			
3T	5	0	1
1.5T	27	28	48
T1-weighted	32	26	48
2D T1-weighted	28	25	7
3D T1-weighted	4	1	41
T2-weighted	30	27	29
T1- and T2-weighted	30	25	27

wingless-type [WNT], group 3, and group 4) with specific subgroups conferring important prognostic and therapeutic differences.[2-4] For example, patients with WNT-pathway-activated tumors have favorable outcomes with a nearly 90% 5-year survival rate, while patients with group 3 tumors have <50% overall survival.[5] These divergent prognostic outcomes have propelled the recognition of these 4 subgroups, reflected in the recent revision of the World Health Organization classification of MB.[6] These molecular subgroups now drive risk-stratification, clinical outcome modeling, and novel therapeutic development.[7,8]

Subtyping of tumors is frequently performed on tissues obtained from surgical resection but can also be performed from tissues obtained from a single biopsy. Even single biopsies of MB can yield accurate information for subtyping because of the presence of spatially homogeneous transcriptomes in MBs, in contrast to other tumor types such as high-grade gliomas.[9] However, surgical sampling is invasive and confers added risk to patients. In addition, despite the increasing clinical utility of MB subtyping, the translation of these genomic insights into clinical practice has been limited by extensive cost and a lack of access to sophisticated methods for accurate and expedient subgroup/subtype analyses.[3]

Radiomics is an emerging discipline that can link imaging features to tumor genotype and serves as a promising approach to identify surrogate biomarkers that can accurately reflect tumor genomics.[10] Radiomic strategies have been extensively investigated in multiple cancer types, including non-small cell lung cancer,[11] glioblastoma,[12-16] hepatocellular carcinoma,[17] prostate cancer,[18] and breast cancer.[19] However, few studies have applied radiomics to MB; in those that have, the focus has been on the qualitative characterization of these tumors on MR imaging.[20-26] Specifically, these studies have shown that tumor location and enhancement patterns differ across MB subgroups.[20-24,26] For example, group 3 and group 4 MBs often arise in the midline, SHH tumors occur most frequently in the cerebellar hemispheres, and WNT tumors occur in both the midline and the cerebellar peduncle/cerebellopontine angle cistern locations.[20,22-24] Moreover, absence of enhancement is predictive of group 4 tumors,[23] while extensive enhancement in non-WNT/SHH tumors is predictive of poorer overall and event-free survival.[21] While qualitative image features of MB subgroups can provide useful clinical insight, they are subject to interobserver variability and do not capture all the multidimensional data that are acquired by MR imaging.

To date, the use of a quantitative imaging approach for the predictive analysis of MB subgroups has not yet been well-developed. In this multi-institutional study, we aimed to develop and validate radiomic and machine-learning methods to identify computational MR image signatures that are predictive of distinct molecular subgroups of MB. The discovery and establishment of noninvasive and surrogate imaging markers of MB subgroups can provide clinicians with a window into the genomics of these tumors, which can ultimately be helpful for clinical prognostication and informing management.

MATERIALS AND METHODS

Patients

This multicenter retrospective study was approved by the institutional review board or research ethics board from each of the 3 participating academic institutions: Lucile Packard Children's Hospital (Stanford University, Palo Alto, California), Boston Children's Hospital (Boston, Massachusetts), and the Hospital for Sick Children (Toronto, Ontario, Canada). Because this was a retrospective study, informed consent was waived. Interinstitutional data agreement was obtained for data-sharing. All patients with de novo and histologically confirmed MBs were identified from the medical record data base of each institution from January 2001 to January 2014. These patients were further screened using the following inclusion criteria: availability of high-quality preoperative MR imaging as determined by experienced pediatric neuroradiologists, neurosurgeons, and neuro-oncologists and the availability of molecular subgroup information or the availability of tumor tissue for molecular subtyping. A total of 109 patients were included across the 3 institutions (Lucile Packard Children's Hospital, $n = 32$; Boston Children's Hospital, $n = 28$; the Hospital for Sick Children, $n = 49$), comprising 64 males and 45 females; mean age, 8.56 ± 5.75 years; range, 1–18 years (Table 1). Clinicopathologic information including age, sex, histology diagnosis, and molecular subgroups, if available, was obtained from the medical record.

Molecular Analysis

Four distinct MB molecular subgroups (WNT, SHH, group 3, and group 4) were identified on the basis of gene-expression profiling using a nanoString-based assay (http://www.nanostring.com) as previously described.[27] For most patients, molecular analysis was performed with formalin-fixed paraffin-embedded tissue that was obtained at the time of surgical diagnosis. A small number of patients had molecular subtyping based on frozen tissue.

MR Imaging Acquisition, Image Data Retrieval, and Image Segmentation

All patients from Lucile Packard Children's Hospital/Stanford University underwent brain MR imaging at 1.5T or 3T (Signa or

Discovery 750; GE Healthcare, Milwaukee, Wisconsin). MRIs were performed using the brain tumor protocol of the institution, which included 2D axial T2-weighted spin-echo (TR/TE, 2500–5600/80–110 ms; 4- to 5-mm slice thickness; 0- to 1.5-mm skip), 2D axial or sagittal precontrast T1-weighted spin-echo, and 2D axial gadolinium-enhanced T1-weighted spin-echo (TR/TE, 400–1000/8–21 ms; 2- to 5-mm slice thickness; 0- to 1.5-mm skip) sequences. Four patients had 3D T1-weighted spoiled gradient recalled-echo (TR/TE, 8/3 ms; 1-mm slice thickness; 0-mm skip) instead of 2D T1-weighted spin-echo imaging. Patients from Boston Children's Hospital all underwent 1.5T brain MR imaging (Signa; GE Healthcare). Sequences acquired included 2D axial T2-weighted spin-echo (TR/TE, 3000–5000/80–100 ms; 4- to 5-mm slice thickness; 0- to 1.5-mm skip), 2D axial precontrast T1-weighted spin-echo, and 2D axial gadolinium-enhanced T1-weighted spin-echo (TR/TE, 500–700/8–22 ms; 4- to 6-mm slice thickness; 0- to 1.5-mm skip). One patient had 3D T1-weighted spoiled gradient recalled-echo (TR/TE, 8/2 ms; 1.5-mm slice thickness; 0-mm skip) instead of 2D T1-weighted spin-echo imaging. Patients from the Hospital for Sick Children underwent brain MR imaging at 1.5T or 3T across various scanner vendors (Signa, GE Healthcare; Achieva, Philips Healthcare Best, the Netherlands; Avanto, Siemens, Erlangen, Germany). Sequences acquired included 2D axial T2-weighted fast spin-echo (TR/TE, 3000–6800/80–120 ms; 3- to 6-mm slice thickness; 0.5- to 2.5-mm skip) and, in contrast to the other 2 cohorts, 3D axial precontrast and 3D axial gadolinium-enhanced T1-weighted turbo or fast-field echo (TR/TE, 5–11/2–5 ms; 1- to 2-mm slice thickness; 0-mm skip) sequences were acquired in most patients. Seven patients had 2D T1-weighted fast spin-echo (TR/TE, 8/2 ms; 1.5-mm slice thickness; 0-mm skip) instead of 3D T1-weighted turbo or fast-field echo imaging. All MR imaging data were extracted from the PACS at each respective institution and were subsequently de-identified for compliance with the Health Insurance Portability and Accountability Act before any analyses occurred.

An experienced team of radiologists supervised by a board-certified neuroradiologist with ≥10 years of experience in pediatric neuro-oncology imaging (T.Y.P.) manually drew ROIs around the tumor margin via a quantitative imaging informatics platform, electronic Physician Annotation Device (ePAD, https://epad.stanford.edu). Radiologists annotated on each contiguous image slice where the tumor was present on T2-weighted and contrast-enhanced T1-weighted images. The presence of tumor enhancement was confirmed by comparing precontrast with postcontrast T1-weighted images. Areas of intrinsic T1-hyperintensity (T1 signal that was present on precontrast images and likely representative of blood) were excluded from the final tumor ROIs. Final and proper placement of ROIs was confirmed by another board-certified neuroradiologist with ≥10 years of experience in pediatric neuro-oncology imaging (K.W.Y.).

Radiomic Feature-Extraction Methodology

We developed a computational framework to capture a variety of phenotypic characteristics of tumor. A total of 590 MR imaging–based radiomic features were extracted from the ROIs on T2-weighted and contrast-enhanced T1-weighted MR images, respectively. The primary types of radiomic features included intensity-based histograms, tumor edge-sharpness, Gabor features, and local area integral invariant (LAII) (all features used are described in On-line Tables 1 and 2). The Daube on Histogram features were based on Daubechies wavelet decomposition. The Quantitative Image-Feature Engine[28] offers additional detailed definitions of the extracted radiomic features (On-line Table 1). The *z* score normalization was used on each feature to standardize the range of all image features.

Statistical Analysis

Statistical analysis was conducted with Python software (2.7.14, https://www.python.org/). A nonparametric Wilcoxon rank sum test was used for feature selection, and a support vector machine (SVM) classifier was used for prediction. Statistical significance levels were all 2-sided, with statistical significance set at $P < .05$. Receiver operating characteristic (ROC) curve analysis was used to perform prediction evaluation of each molecular subgroup of MB.

Feature Selection, Radiomics, and Machine Learning Approach

The feature-selection method was applied to select the most discriminative features within a 10-fold cross-validation evaluation strategy (see "Model Evaluation"). Specifically, we used the Wilcoxon rank sum test[29] on individual features and sorted them by the acquired *P* values. After cross-validation analysis, the top k (k = 5, 10, 15, 20, 30, 40, 50, 100, 200, and 300) features with smallest k *P* values were selected in the training set. We then assessed the predictive power of selected radiomic features on the validation set.

We applied the SVM classifier using a double 10-fold cross-validation strategy for testing the performance of the model in predicting the 4 main MB molecular subgroups. SVM tackles high-dimensional data classification by weighting features and the use of a Gaussian radial basis function kernel. During the training process, to avoid potential overfitting, we determined the optimal parameters of the SVM classifier and the optimal number of image features using an internal 10-fold cross-validation and tested them by a range of selected features (top 5, 10, 15, 20, 30, 40, 50, 100, 200, and 300 features). Next, the trained model with the best area under the receiver operating characteristic curve (AUC) value was used for testing unseen samples in an outer 10-fold cross-validation strategy to determine the test set performance.

Model Evaluation

Two validation schemes were incorporated to evaluate the predictive performance of extracted radiomic features. To determine the generalization accuracy of the predictive models, we first performed a double 10-fold cross-validation on a single dataset containing all 3 patient cohorts (Fig 1). To validate the model across different institutions, we next tested an evaluation strategy in which we trained the model using the combined dataset from 2 institutions; then, we tested the model on data from the third independent institution. This process was repeated 3 times with each institutional cohort serving once as the test set (Fig 1), allow-

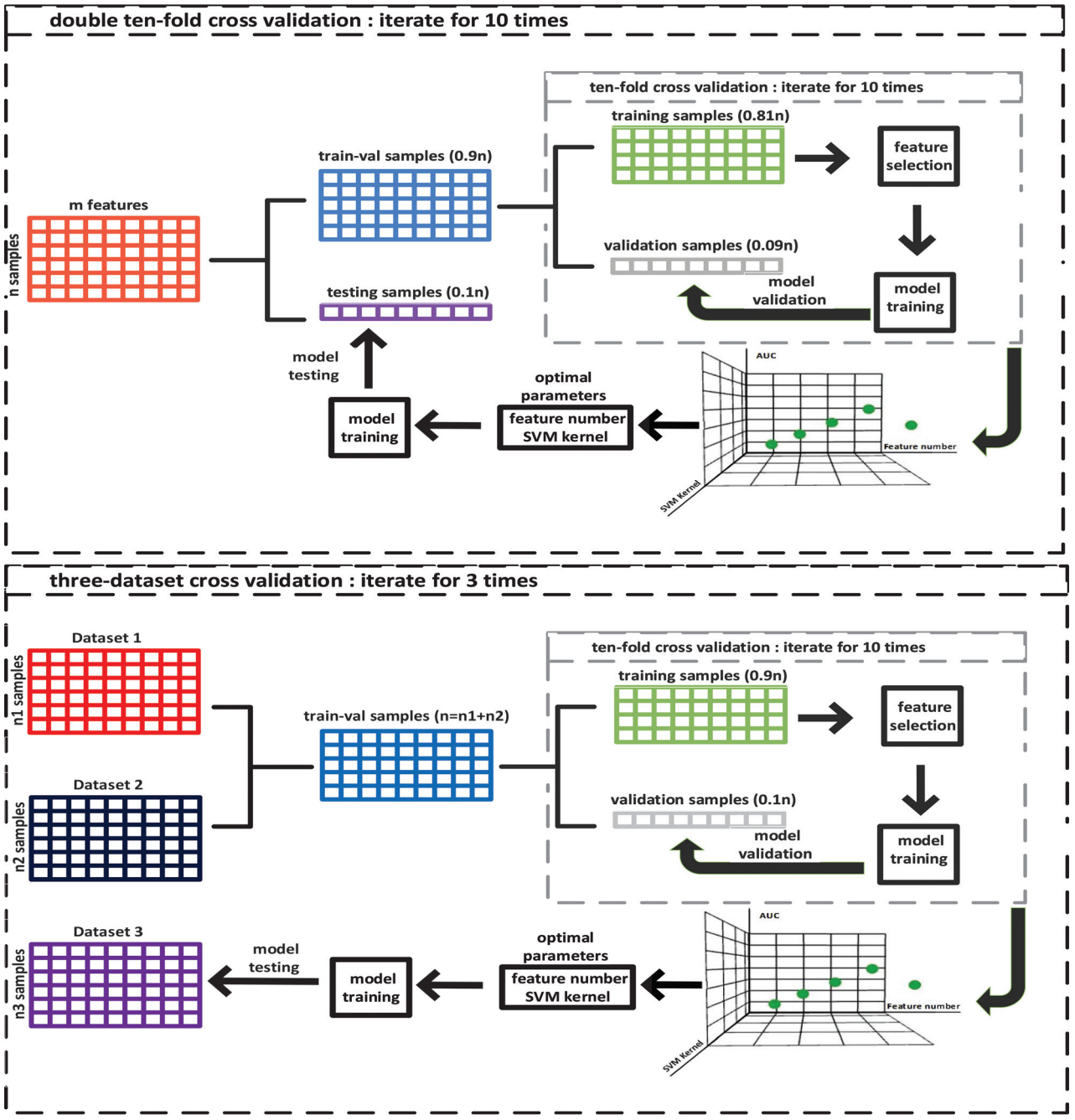

FIG 1. Illustration of 2 strategies used to evaluate the supervised machine learning models to predict the molecular subgroups of medulloblastoma. The upper and lower figures show details of double 10-fold cross-validation and 3-dataset cross-validation schemes, respectively.

ing us to evaluate truly predictive radiomic features across clinical sites with different vendors and imaging parameters. The overall model performance was assessed using the average of the 3 iterations and by determination of the AUC.

RESULTS

Model Evaluation

Table 2 summarizes the mean AUCs for prediction of the MB subgroups using the double 10-fold cross-validation and 3-dataset cross-validation strategies on solely T1-weighted, solely T2-weighted, and combined T1- and T2-weighted image datasets.

The double 10-fold cross-validation strategy, which combines all institutional cohorts into 1 dataset, showed that SVMs resulted in the best performance for predicting molecular subgroups. ROC analysis revealed superior performance of this model for predicting the SHH, group 3, and group 4 tumors, particularly when using extracted quantitative data from both T1- and T2-weighted images (AUC = 0.79, 0.70, and 0.83, respectively) (Fig 2). In contrast, the model was not strongly predictive of WNT tumors, despite using all the different image types (AUC = 0.45–0.63).

Fig 3 shows ROC curves of the best models for each MB subgroup obtained with our second validation scheme (independent 3-dataset cross-validation) (See On-line Fig 1 for all ROC curves). While not strongly predictive of group 3 tumors, the computa-

tional features extracted from T1-weighted images and the combined dataset from T1- and T2-weighted images were predictive of SHH (AUC = 0.73 and 0.70, respectively) and group 4 (AUC = 0.76 and 0.80, respectively) tumors (Table 2). In addition, while the mean AUC for predicting WNT tumors using T2-weighted images was good (0.72), there were institutional differences in performance (Stanford, AUC = 0.90; Boston, AUC = 0.49; Toronto, AUC = 0.76), suggesting that more training samples of the WNT group are needed to yield stable prediction outcomes.

Identification of Discriminative Radiomic Features

To identify discriminative radiomic features for predicting the 4 main molecular subgroups of MB (Fig 4) within our study population, we analyzed the results of selected features for all tested models. On-line Table 3 shows the best number of features for each institutional cohort and the number of overlapping features that was selected in all 3 cross-validation loops (see On-line Table 4 for a complete list of feature categories and the number of overlapped features in each category). We observed that the prediction of SHH is the most robust across all institutions because the optimal feature number for 3 cross-validation loops is the same (40 features), which represented a small subset of all 590 features (6.8%). Of all the features evaluated, there were 4 leading categories: lesion area, edge-sharpness, LAII, and histogram features (On-line Fig 2), with edge-sharpness features being the most important for predicting SHH and group 4.

Table 2: Predictive performance of 2 machine learning models for the identification of medulloblastoma molecular subgroups

MRI Dataset/Targeted Subgroup	AUC with Double 10-Fold Cross-Validation	AUC with 3-Dataset Cross-Validation
T1		
SHH	0.67	0.73
WNT	0.56	0.47
Group 3	0.40	0.54
Group 4	0.79	0.76
T2		
SHH	0.70	0.66
WNT	0.63	0.72
Group 3	0.51	0.57
Group 4	0.54	0.59
T1 + T2		
SHH	0.79	0.70
WNT	0.45	0.45
Group 3	0.70	0.39
Group 4	0.83	0.80

DISCUSSION

In this study, we developed and validated radiomic and machine learning approaches to identify individual categories of MR imaging–based radiomic features that predict distinct biologic subgroups of MB. Our first method using the double 10-fold cross-validation scheme allowed the prediction of SHH and group 4 tumors using combined information extracted from T1- and T2-weighted sequences, which are frequently acquired as part of the brain tumor MR imaging protocol of any institution. The second method using an independent 3-dataset cross-validation scheme showed the potential for applying our computational pipeline to datasets from outside institutions. In keeping with the results of our first method, this approach yielded a good predictive performance of SHH and group 4 tumors using combined T1 and T2 datasets. However, both models performed comparatively less robustly in predicting WNT and group 3 tumors, perhaps related to the lower amount of available imaging data for these specific subgroups and more molecular heterogeneity across group 3 tumors.

Several brain tumors are known to have spatial molecular[1,9,30,31] and imaging[13,22,23,25,26] heterogeneity. With regard to MB, the identification of 4 molecular subgroups in the past decade has deepened our understanding of the underlying biology of this tumor and the correlation of a specific tumor genotype with different clinical outcomes.[2,3,5] A recent study analyzing multiple biopsies within MB showed that a single biopsy can accurately and reliably subtype MB due to its spatially homogeneous transcriptomes, in contrast to the markedly heterogeneous genomic landscape of glioblastomas; however, actionable somatic mutations found in a single biopsy of MB were infrequently clonal across the entire tumor, which underscores the true molecular heterogeneity of this tumor.[9] In fact, Cavalli et al[32] have further identified 12 distinct subtypes within each of the 4 core MB subgroups, each with differing clinical presentations, prognosis, and copy-number mutations. Thus, the complex molecular heterogeneity of MB subgroups and the paucity of imaging data available for individual subgroups in this study may help to explain the performance of our models for predicting WNT and group 3 tumors. Additionally, prior studies have shown tumor location to be a unique factor, particularly for predicting WNT tumors,[22-24] and radiomic analysis of isolated tumor volume may be another explanation for our model performance. Thus, the incorporation of qualitative semantic features such as tumor location into our model may improve its performance, particularly for the prediction of WNT medulloblastomas, which is important clinically be-

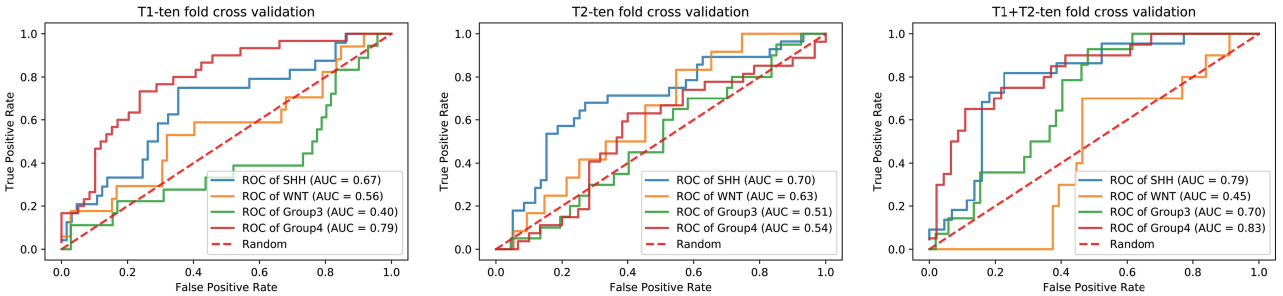

FIG 2. Receiver operating characteristic curves with a double 10-fold cross-validation scheme for support vector machine to predict the 4 main molecular subgroups of medulloblastoma with the use of computational MR imaging features.

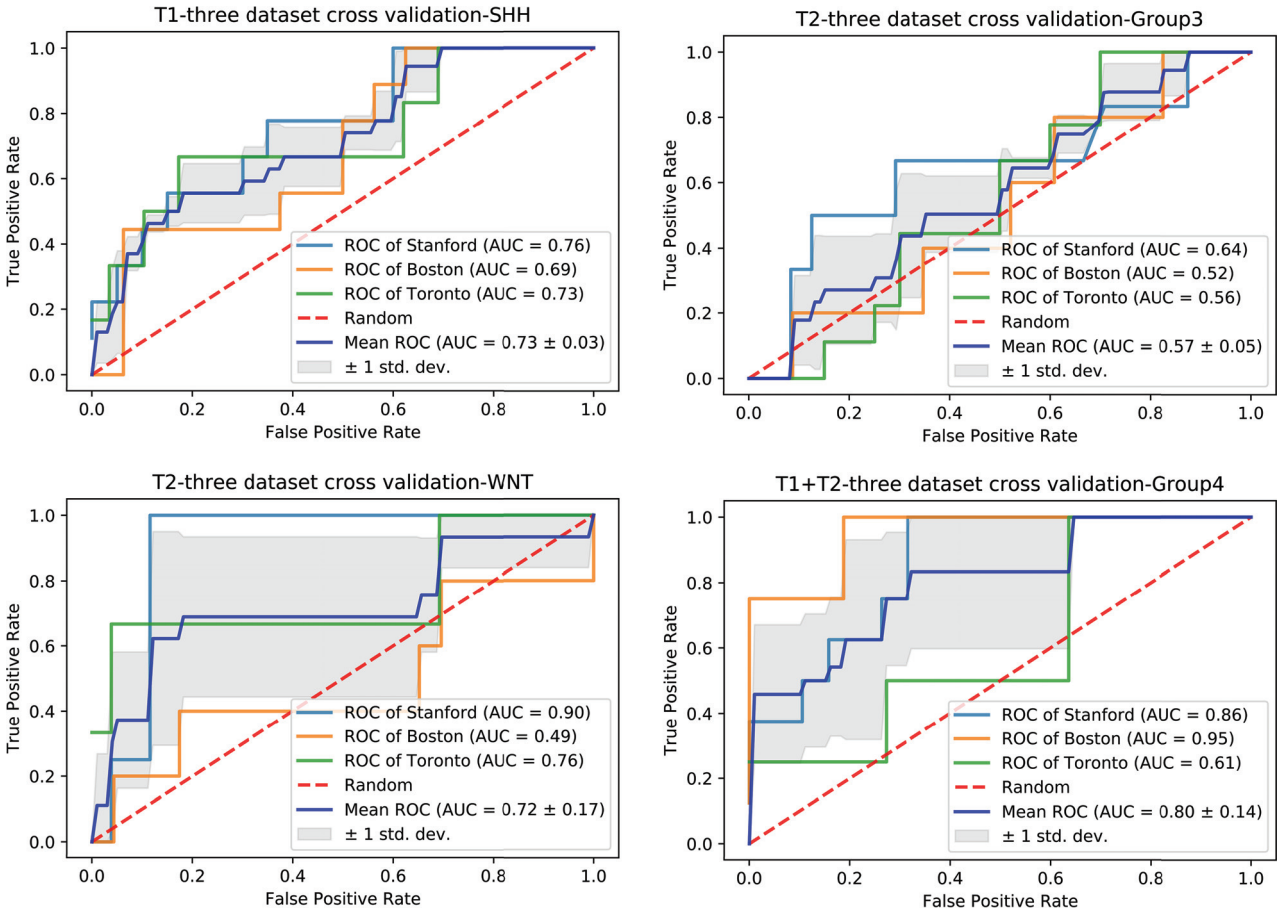

FIG 3. Receiver operating characteristic curves with the largest mean AUC values for 4 distinct molecular subgroups of medulloblastoma with a 3-dataset cross-validation scheme.

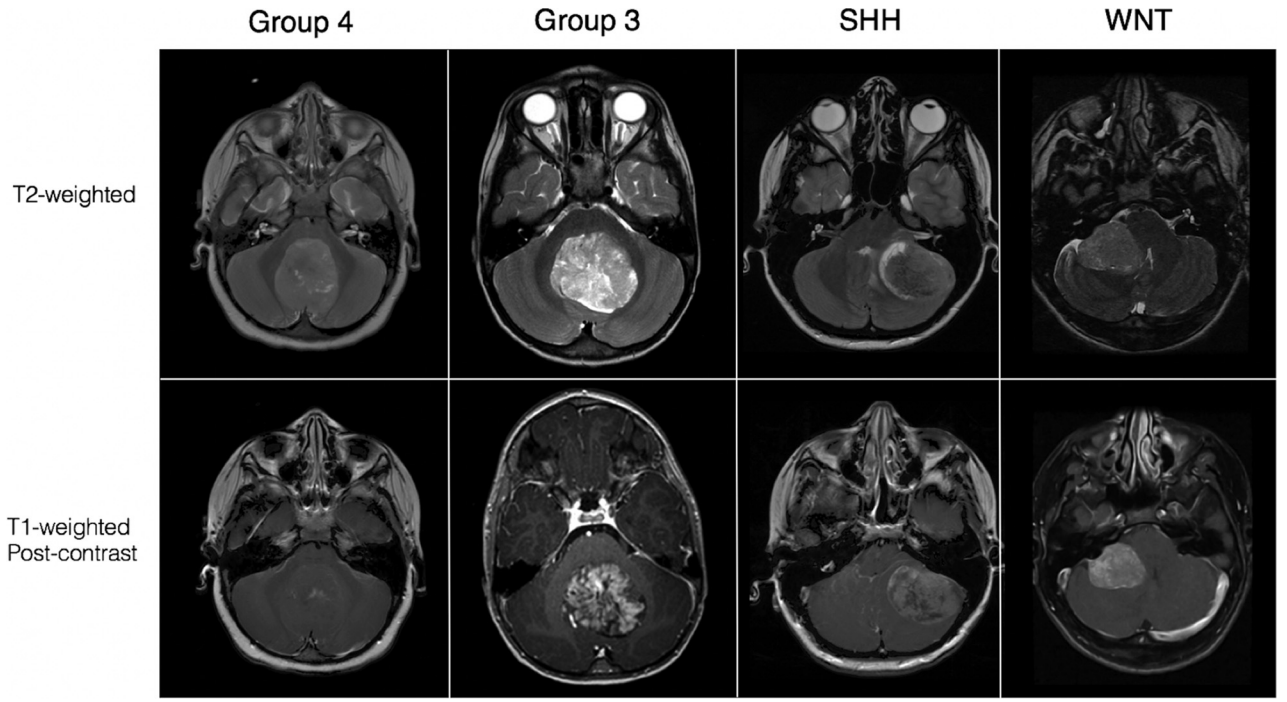

FIG 4. MR imaging appearance of the 4 core molecular subgroups of medulloblastoma on T2-weighted and contrast-enhanced T1-weighted images.

cause this subgroup is associated with the best prognosis and may not need the aggressive therapies used to treat other subgroups.[4]

Because MR imaging has the capacity to capture the structure and physiology of an entire tumor, it can be an invaluable tool for noninvasively evaluating tumoral genetic heterogeneity.[33] The spatial variations in genetic and molecular expression of MBs can manifest as different imaging phenotypes on MR imaging, with varying degrees of intratumoral enhancement, hemorrhage, and signal intensity on T1- and T2-weighted images.[16,21-23,25,26] Radiomic studies, most of which have focused on adult glioblastomas, have shown success in linking quantitative imaging features with key mutations as well as clinical outcomes.[12-14,34-36] For example, 1 study proposed that a distinct glioblastoma subtype, specifically, a rim-enhancing cluster found to upregulate the vascular endothelial growth factor receptor signaling pathway, is more likely to respond to upfront antiangiogenic therapy.[12] Many genetic factors (eg, *MYC*, *MYCN*, *OTX2*, *CDK6*, *SNCAIP*, and *ACVR1*) contribute to the 4 main MB subgroups and associated prognostic differences; even within the SHH and group 3 subgroups, more granular sub-subgroups have emerged with significant differences in the rate of metastases and 5-year survival.[32,37] Given molecular complexities that pose challenges in MB subclassification, there is an important future role for a high-performance, image-based biomarker that either predicts such unique molecular groups or subgroups of MB or provides a more robust tumor risk-stratification scheme for treatment decision-making independent of molecular grouping or subgrouping.

Furthermore, a rapid, low-risk, and inexpensive platform for classifying MB that is feasible with radiomic and machine learning algorithms can potentially enable more widespread tumor subtyping in clinical institutions that may have limited histopathologic and genomic resources. While immunohistochemistry markers (*GAB1*, β-catenin, filamin A, and *YAP1*) are currently used in some institutions to identify SHH and WNT tumors, identifying specific group 3 or group 4 tumors remains expensive and difficult without the application of gene expression or methylation profiling.[38,39] In this study, we show a relatively high performance for predicting group 4 MB that is feasible with a computational analysis scheme.

This study has limitations. Because this was a retrospective and multi-institutional study, there was heterogeneity in MR image data, including the use of different scanner vendors and imaging parameters. However, in clinical practice, different scanner vendors at different field strengths and different imaging protocols are used daily for tumor diagnosis and surveillance; thus, a predictive model that incorporates such technical variations results in a more practical clinical translation of radiogenomic strategies. A recent study showed that radiomic features varied considerably on T1-weighted images generated by different pulse sequences and parameters.[40] In this study, we chose to retain differences in imaging protocols from 3 different cohorts to assess the robustness of radiomic features extracted from multi-institutional data. To facilitate evaluation of classifiers, after feature extraction, we performed feature-level normalization (z score) across patients to help with the predictive performance of the machine learning classifier. Future studies may need to look into other strategies to overcome the heterogeneity of data, including normalizing the degree of T1-weighting (eg, normalizing images to the signal intensity of the tumor) and weighting the importance of specific features or image sequences (eg, T1 versus T2) as input in a predictive radiogenomic model.[40] In addition, while this study used T1 contrast-enhanced and T2-weighted images for feature discrimination and model development, incorporating additional image sequences, such as diffusion, permeability, or T2* perfusion, could further boost model performance. Despite these challenges, our study showed that radiomic strategies can be used to extract discriminating computational features and create a machine learning–based prediction model for pediatric MB subgroups.

CONCLUSIONS

We present proof-of-concept results for the application of radiomics and machine learning using multi-institutional data for the prediction of distinct MB molecular subgroups. High-throughput quantitative features were extracted from contrast-enhanced T1- and T2-weighted images and linked to 4 core subgroups of MB. Model performance for the prediction of SHH and group 4 was more robust than for WNT and group 3. Future investigations using a larger sample size for all subgroups, particularly WNT (because we had the least amount of WNT cases in this study), is needed to improve classifier training and evaluation during cross-validation. The use of other imaging sequences such as diffusion-weighted, permeability, and T2* perfusion imaging may also yield additional radiomic features and help to improve performance. Computational analyses of MR imaging offer a wealth of opportunities to noninvasively characterize tumors, which can have an important role in the clinical and treatment decision-making processes for pediatric MB.

Disclosures: Paul G. Fisher—*UNRELATED*: *Employment*: Elsevier Publishing, *Comments*: stipend of $22,500 per year for work as Associate Editor for the *Journal of Pediatrics*; *Grants/Grants Pending*: National Institutes of Health, *Comments*: salary support from the National Cancer Institute (Pediatric Brain Tumor Consortium) and from the National Human Genome Research Institute (Undiagnosed Diseases Consortium).* Vijay Ramaswamy—*RELATED*: *Grant*: collaborative ependymoma research network. Tina Young Poussaint—*UNRELATED*: *Grants/Grants Pending*: National Institutes of Health, Pediatric Brain Tumor Consortium Neuroimaging Center.* Olivier Gevaert—*RELATED*: *Grant*: National Institutes of Biomedical Imaging and Bioengineering, *Comments*: Research reported in this publication was supported by the National Institute of Biomedical Imaging and Bioengineering of the National Institutes of Health under Award Number R01EB020527. The content is solely the responsibility of the authors and does not necessarily represent the official views of the National Institutes of Health*; *UNRELATED*: *Grants/Grants Pending*: National Institutes of Health, *Comments*: support from various grants from the National Institutes of Health, and foundation grant from the Innovation in Cancer Informatics fund.* *Money paid to the institution.

REFERENCES

1. Pollack IF, Jakacki RI. **Childhood brain tumors: epidemiology, current management and future directions.** *Nat Rev Neurol* 2011;7:495–506 CrossRef Medline
2. Kool M, Korshunov A, Remke M, et al. **Molecular subgroups of medulloblastoma: an international meta-analysis of transcriptome, genetic aberrations, and clinical data of WNT, SHH, group 3, and group 4 medulloblastomas.** *Acta Neuropathol* 2012;123:473–84 CrossRef Medline
3. Northcott PA, Korshunov A, Witt H, et al. **Medulloblastoma comprises four distinct molecular variants.** *J Clin Oncol* 2011;29:1408–14 CrossRef Medline
4. Taylor MD, Northcott PA, Korshunov A, et al. **Molecular subgroups**

of medulloblastoma: the current consensus. *Acta Neuropathol* 2012; 123:465–72 CrossRef Medline
5. Ramaswamy V, Remke M, Bouffet E, et al. **Risk stratification of childhood medulloblastoma in the molecular era: the current consensus.** *Acta Neuropathol* 2016;131:821–31 CrossRef Medline
6. Louis DN, Perry A, Reifenberger G, et al. **The 2016 World Health Organization Classification of Tumors of the Central Nervous System: a summary.** *Acta Neuropathol* 2016;131:803–20 CrossRef Medline
7. Gajjar AJ, Robinson GW. **Medulloblastoma-translating discoveries from the bench to the bedside.** *Nat Rev Clin Oncol* 2014;11:714–22 CrossRef Medline
8. Archer TC, Mahoney EL, Pomeroy SL. **Medulloblastoma: molecular classification-based personal therapeutics.** *Neurotherapeutics* 2017; 14:265–73 CrossRef Medline
9. Morrissy AS, Cavalli FM, Remke M, et al. **Spatial heterogeneity in medulloblastoma.** *Nat Genet* 2017;49:780–88 CrossRef Medline
10. Zhou M, Scott J, Chaudhury B, et al. **Radiomics in brain tumor: image assessment, quantitative feature descriptors, and machine-learning approaches.** *AJNR Am J Neuroradiol* 2018;39:208–16 CrossRef Medline
11. Gevaert O, Xu J, Hoang CD, et al. **Non-small cell lung cancer: identifying prognostic imaging biomarkers by leveraging public gene expression microarray data–methods and preliminary results.** *Radiology* 2012;264:387–96 CrossRef Medline
12. Itakura H, Achrol AS, Mitchell LA, et al. **Magnetic resonance image features identify glioblastoma phenotypic subtypes with distinct molecular pathway activities.** *Sci Transl Med* 2015;7:303ra138 CrossRef Medline
13. Gevaert O, Mitchell LA, Achrol AS, et al. **Glioblastoma multiforme: exploratory radiogenomic analysis by using quantitative image features.** *Radiology* 2014;273:168–74 CrossRef Medline
14. Kickingereder P, Bonekamp D, Nowosielski M, et al. **Radiogenomics of glioblastoma: machine learning-based classification of molecular characteristics by using multiparametric and multiregional MR imaging features.** *Radiology* 2016;281:907–18 CrossRef Medline
15. Jamshidi N, Diehn M, Bredel M, et al. **Illuminating radiogenomic characteristics of glioblastoma multiforme through integration of MR imaging, messenger RNA expression, and DNA copy number variation.** *Radiology* 2014;270:1–2 CrossRef Medline
16. Zhou M, Chaudhury B, Hall LO, et al. **Identifying spatial imaging biomarkers of glioblastoma multiforme for survival group prediction.** *J Magn Reson Imaging* 2017;46:115–23 CrossRef Medline
17. Banerjee S, Wang DS, Kim HJ, et al. **A computed tomography radiogenomic biomarker predicts microvascular invasion and clinical outcomes in hepatocellular carcinoma.** *Hepatology* 2015;62:792–800 CrossRef Medline
18. Stoyanova R, Takhar M, Tschudi Y, et al. **Prostate cancer radiomics and the promise of radiogenomics.** *Transl Cancer Res* 2016;5:432–47 CrossRef Medline
19. Grimm LJ. **Breast MRI radiogenomics: current status and research implications.** *J Magn Reson Imaging* 2016;43:1269–78 CrossRef Medline
20. Gibson P, Tong Y, Robinson G, et al. **Subtypes of medulloblastoma have distinct developmental origins.** *Nature* 2010;468:1095–99 CrossRef Medline
21. Lastowska M, Jurkiewicz E, Trubicka J, et al. **Contrast enhancement pattern predicts poor survival for patients with non-WNT/SHH medulloblastoma tumours.** *J Neurooncol* 2015;123:65–73 CrossRef Medline
22. Patay Z, DeSain LA, Hwang SN, et al. **MR imaging characteristics of wingless-type-subgroup pediatric medulloblastoma.** *AJNR Am J Neuroradiol* 2015;36:2386–93 CrossRef Medline
23. Perreault S, Ramaswamy V, Achrol AS, et al. **MRI surrogates for molecular subgroups of medulloblastoma.** *AJNR Am J Neuroradiol* 2014;35:1263–69 CrossRef Medline
24. Teo WY, Shen J, Su JM, et al. **Implications of tumor location on subtypes of medulloblastoma.** *Pediatr Blood Cancer* 2013;60: 1408–10 CrossRef Medline
25. Yeom KW, Mobley BC, Lober RM, et al. **Distinctive MRI features of pediatric medulloblastoma subtypes.** *AJR Am J Roentgenol* 2013; 200:895–903 CrossRef Medline
26. Zhao F, Li C, Zhou Q, et al. **Distinctive localization and MRI features correlate of molecular subgroups in adult medulloblastoma.** *J Neurooncol* 2017;135:353–60 CrossRef Medline
27. Northcott PA, Shih DJ, Remke M, et al. **Rapid, reliable, and reproducible molecular sub-grouping of clinical medulloblastoma samples.** *Acta Neuropathol* 2012;123:615–26 CrossRef Medline
28. Echegaray S, Bakr S, Rubin DL, et al. **Quantitative Image Feature Engine (QIFE): an open-source, modular engine for 3D quantitative feature extraction from volumetric medical images.** *J Digit Imaging* 2018;31:403–14 CrossRef Medline
29. Wilcoxin F. **Probability tables for individual comparisons by ranking methods.** *Biometrics* 1947;3:119–22 CrossRef Medline
30. Pajtler KW, Witt H, Sill M, et al. **Molecular classification of ependymal tumors across all CNS compartments, histopathological grades, and age groups.** *Cancer Cell* 2015;27:728–43 CrossRef Medline
31. Northcott PA, Buchhalter I, Morrissy AS, et al. **The whole-genome landscape of medulloblastoma subtypes.** *Nature* 2017;547:311–17 CrossRef Medline
32. Cavalli FM, Remke M, Rampasek L, et al. **Intertumoral heterogeneity within medulloblastoma subgroups.** *Cancer Cell* 2017;31:737–54.e6 CrossRef Medline
33. Gatenby RA, Grove O, Gillies RJ. **Quantitative imaging in cancer evolution and ecology.** *Radiology* 2013;269:8–15 CrossRef Medline
34. Kickingereder P, Neuberger U, Bonekamp D, et al. **Radiomic subtyping improves disease stratification beyond key molecular, clinical and standard imaging characteristics in patients with glioblastoma.** *Neuro Oncol* 2018;20:848–57 CrossRef Medline
35. Grossmann P, Narayan V, Chang K, et al. **Quantitative imaging biomarkers for risk stratification of patients with recurrent glioblastoma treated with bevacizumab.** *Neuro Oncol* 2017;19:1688–97 CrossRef Medline
36. Hu LS, Ning S, Eschbacher JM, et al. **Radiogenomics to characterize regional genetic heterogeneity in glioblastoma.** *Neuro Oncol* 2017; 19:128–37 CrossRef Medline
37. Northcott PA, Shih DJ, Peacock J, et al. **Subgroup-specific structural variation across 1,000 medulloblastoma genomes.** *Nature* 2012;488: 49–56 CrossRef Medline
38. Lastowska M, Trubicka J, Niemira M, et al. **Medulloblastoma with transitional features between group 3 and group 4 is associated with good prognosis.** *J Neurooncol* 2018;138:231–40 CrossRef Medline
39. Ellison DW, Dalton J, Kocak M, et al. **Medulloblastoma: clinicopathological correlates of SHH, WNT, and non-SHH/WNT molecular subgroups.** *Acta Neuropathol* 2011;121:381–96 CrossRef Medline
40. Ford J, Dogan N, Young L, et al. **Quantitative radiomics: impact of pulse sequence parameter selection on MRI-based textural features of the brain.** *Contrast Media & Molecular Imaging* 2018. https://doi.org/10.1155/2018/1729071. Accessed August 16, 2018